Effect of pre-main-post diesel injection strategy on greenhouse gas and nitrogen oxide emissions of natural gas/diesel dual-fuel engine at high load conditions

Yousefi, Amin; Guo, Hongsheng; Dev, Shouvik; Liko, Brian; Lafrance, Simon

Publisher's version / Version de l'éditeur:
https://doi.org/10.1016/j.fuel.2021.121110
Fuel, 302, 15 October 2021, pp. 1-13, 2021-05-29

Effect of pre-main-post diesel injection strategy on greenhouse gas and nitrogen oxide emissions of natural gas/diesel dual-fuel engine at high load conditions

Amin Yousefi*, Hongsheng Guo, Shouvik Dev, Brian Liko, Simon Lafrance

Energy, Mining, and Environment Research Center, National Research Council Canada, 1200 Montreal Road, Ottawa, Ontario K1A 0R6, Canada

Abstract

Natural gas/diesel dual-fuel (NDDF) engine technology is an interesting concept for decreasing greenhouse gas (GHG) emissions of heavy-duty diesel engines. One of the main limitations of this concept is the emissions of unburned methane which is estimated to have a GHG potential factor of 25 – 34 over a 100-year period. Our previous study has shown that a NDDF engine using pre-main-post diesel injection strategy can reduce unburned methane emissions compared to that using single diesel injection strategy under high engine load conditions. However, it yields lower indicated thermal efficiency (ITE) and higher carbon dioxide (CO_2) and nitrogen oxides (NO_x) emissions due to the advanced combustion phasing. In this study, the combustion phasing of pre-main-post diesel injection strategy is further optimized with the goal to improve the ITE and reduce the GHG and NO_x emissions without compromising the unburned methane emissions when compared to single injection strategy. The results reveal that changing pre diesel injection timing gives more controllability of the combustion phasing than changing the main and post diesel injection timing. A more homogenous premixed mixture of pre injected diesel – natural gas – air retards the combustion phasing which allowed further improvement of the ITE and GHG emissions of NDDF engines while maintaining the low unburned methane emissions feature of the pre-main-post injection strategy. It is found that the optimized pre-main-post diesel injection strategy is able to reduce unburned methane, GHG, and NO_x emissions by 13.4%, 1.5%, and 42%, respectively, and increase ITE by 0.37% compared to single injection strategy.

***Keywords**: natural gas; diesel; pre-main-post injection strategy; dual-fuel engine; GHG and NO_x emissions.*

1. Introduction

Despite the extensive use of diesel engines in transportation and various other industries over the last century, the future sustainability of the diesel fueled compression ignition (CI) engines is subject to speculation. The reason is that the combustion of diesel fuel still generates significant carbon dioxide (CO_2) emissions and the diffusion

combustion inside the cylinder of diesel engines leads to high levels of nitrogen oxides (NO_x) and particulate matter (PM) emissions. The Paris Agreement on climate change which was adopted in 2015 aims to strengthen the global response to the threat of climate change by "limiting the global average temperature rise to well below 2 degrees Celsius and pursue efforts to limit the increase to 1.5 degrees Celsius" compared to pre-industrial levels [1]. This goal requires an extensive reduction in greenhouse gas (GHG) emissions and signatory nations were requested to show their own numerical goals. For instance, the Government of Canada has committed to a 30% and 80% reduction in GHG emissions by 2030 and 2050, respectively, relative to the recorded emissions in 2005 [2]. This has exerted significant pressure on industries using diesel engines. The technological advancements and continuous improvement of diesel engines and after-treatment devices have significantly reduced the exhaust NO_x and PM emissions of the CI diesel engines over the last couple of decades [3–7]. Moreover, the fact that CI engines are some of the most efficient combustion engines makes them well suited for not only heavy-duty transportation, but also power generation and marine industries. Therefore, despite the surge of electrification and hybridization in light-duty vehicles, it is projected that CI engines will still play a predominant role in major industries until 2050 [8]. However, the urgency to reduce GHG emissions requires additional steps towards the decarbonisation of CI diesel engines. Improvement of engine efficiency and implementation of alternative cleaner fuels seem to be two apparent solutions to this problem.

Natural gas as a low-carbon fuel is potentially a feasible alternative fuel for use in CI engines to replace diesel and meet stringent emission regulations. It is mainly composed of methane (CH_4) which produces lower CO_2 emissions compared to gasoline and diesel when it combusts completely. When compared with other alternative fuels (i.e., ethanol, methanol, hydrogen, biogas, etc.), natural gas has advantages of relatively lower cost, abundant reserves, global distribution network as well as mature infrastructure for storage and delivery. Natural gas/diesel dual-fuel (NDDF) concept enables the utilization of natural gas in existing CI diesel engines [9–13]. In this concept, diesel directly-injected into the engine cylinder provides an ignition source for the premixed natural gas – air mixture. Typically, a conventional diesel engine can be modified into a NDDF engine without significant changes to the original design. The major change is the addition of a natural gas supply system to the stock diesel engine, which slightly increases control complexity of the fueling system [14]. Conventional NDDF engines produce significant amounts of

unburned methane and GHG emissions and demonstrate lower thermal efficiency at low to medium load conditions compared to their counterpart diesel engines [13,15–17]. This is mainly due to the extra lean premixed charge of natural gas – air mixture which causes the flame propagation failure at low to medium load conditions. Several strategies have been investigated to improve the thermal efficiency and unburned methane and GHG emissions of NDDF engines at low to medium load conditions. Advancing diesel injection timing [11,14,16,18–20], increasing diesel injection rail pressure [21–23], using split diesel injection [15,24–27], and stratification of natural gas – air mixture [28–31] have been the most important strategies to achieve these goals.

Several studies have also shown that NDDF engines can achieve comparable or sometimes higher thermal efficiency and lower GHG emissions compared to their counterpart diesel engines under medium to high load conditions [16,32–38]. For instance, Guo et al. [20] examined the effect of natural gas energy fraction on thermal efficiency and CO_2 equivalent (or GHG) emissions of a NDDF engine at high load conditions. They found that the NDDF engine mode achieves higher thermal efficiency and lower CO_2 equivalent (i.e., CO_2 equivalent = $CO_2 + 25 \times CH_4$) emissions than the diesel engine mode. Rimmer et al. [37] compared the combustion performance and exhaust emissions of a NDDF engine mode with those of diesel engine mode at high load conditions. They also reported that the NDDF engine obtains higher thermal efficiency and lower GHG emissions compared to the diesel engine mode at high load conditions [37]. This is due to the fact that the premixed natural gas – air mixture equivalence ratio is high enough to obtain stable flame propagation after its ignition by diesel.

To the best of authors' knowledge, no research effort had been expended towards providing effective measures for further improvement in thermal efficiency and emissions of NO_x, unburned methane, and GHG of NDDF engines at medium to high load conditions. This is mainly because of the already higher thermal efficiency and lower GHG emissions of NDDF engines at medium to high engine load conditions compared to their counterpart diesel engines. However, according to the Phase (II) of Environmental Protection Agency's (EPA's) GHG regulation which starts in 2021, the global warming potential factor for methane will increase from 25 to 34, making the GHG impact of methane emissions more severe [39]. Moreover, for the EPA Tier 4 final of off-road diesel engines for the power generation category of up to 560 kW and above, the NO_x emissions mandate is 0.4 g/kWh [40]. Therefore, developing strategies to simultaneously improve thermal efficiency and reduce emissions of NO_x, unburned methane, and GHG

originating from NDDF engines at medium to high load conditions is also of great importance. In a recent study [10] we proposed a new diesel injection strategy named 'pre-main-post' diesel injection strategy to further reduce the unburned methane emissions of NDDF engines at high load conditions. In this diesel injection strategy, part of the diesel fuel was injected before the main injection during the compression stroke (pre-injection) and part of the diesel fuel was injected after the main injection during the expansion stroke (post-injection). It was found that pre-main-post diesel injection strategy had the potential to decrease the unburned methane emissions of NDDF engines compared to the single diesel injection strategy under high engine load conditions [10]. However, the thermal efficiency of the investigated NDDF engine with pre-main-post diesel injection strategy was lower than that of single diesel injection due to the overly advanced combustion phasing, which leads to higher GHG emissions of pre-main-post diesel injection strategy compared to those of single diesel injection strategy [10].

In this paper the combustion phasing of a NDDF engine with pre-main-post diesel injection strategy is further optimized by tuning the diesel injection timings (i.e., pre, main, and post diesel injection timings) to improve the thermal efficiency and GHG and NO_x emissions of the NDDF engine without compromising the unburned methane emissions compared to the NDDF engine with single diesel injection strategy. A computational fluid dynamic (CFD) model based on CONVERGE 3.0 software is used to simulate the in-cylinder combustion process and help understand the underlying mechanisms of the experimental observations.

2. Experimental setup and methods

2.1. Experimental apparatus

The experimental setup used in this paper is the same as that in our previous paper [10]. A modified single cylinder, four stroke, heavy-duty CAT 3401 base diesel engine is used for the engine tests. Figure 1 shows a schematic of the main components of the experimental setup and Table 1 outlines the relevant specifications of the engine. The engine is coupled with necessary auxiliary systems such as common-rail direct injection (DI) diesel fuel supply systems, charge-air, gaseous port fuel injection (PFI), data acquisition (DAQ) system, as well as exhaust gas emissions analyzer and engine control unit. The common-rail injection system is externally powered by a high-pressure fuel pump and is capable of producing diesel injection pressure up to 1800 bar. A Bronkhorst mini CORI-FLOW mass flow

meter was used to monitor the diesel mass flow rate. A port fuel injection (PFI) system consisting of eight gas injectors (manufactured by Alternative Fuel Systems Inc, Calgary, Alberta) and a Bronkhorst in-flow IP-65 flow meter which measured the flow rate of natural gas were added to introduce natural gas to the engine. National Instruments (NI) hardware (PXI-1031 chassis with PXI-8184 embedded controller) and LabVIEW-based software were used to control the injection timing, pulse width, and injector pressure of both diesel and natural gas.

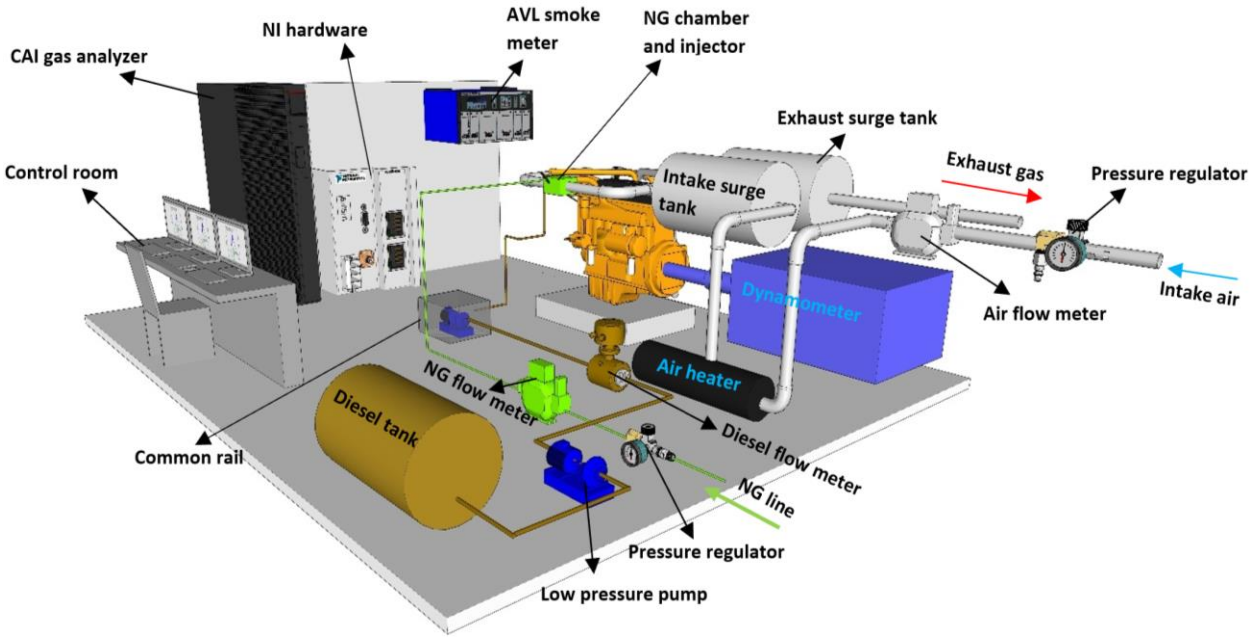

Fig. 1: Schematic of the experimental setup

Table 1. Engine specifications.

Engine model	Caterpillar 3401
Number of cylinders	1
Bore × Stroke (mm × mm)	137.2 × 165.1
Conn. rod length (mm)	261.62
Compression ratio	16.25
Displacement (L)	2.44
Combustion chamber type	Quiescent
Diesel injector	Ganser CRS AG injector
No. diesel injector hole × diameter (mm)	6 × 0.21
Natural gas injector	AFS Inc. GS60 injectors
Maximum power (kW)	74.6 (@ 2100 RPM)
Maximum torque (N.m)	441 (@ 1200 RPM)

The intake charge-air system was equipped with a compressed air supply which supplied a pressure of 5.50 bar to the engine test cell, a Fisher-Emerson control valve to regulate the intake air pressure, a turbine type mass

flowmeter manufactured by Sierra Instruments Inc., and a by-pass heater located upstream of the intake surge tank to provide a desirable intake air temperature. Surge tanks were used before the intake and after the exhaust manifolds to reduce the pressure oscillations during the test. An exhaust back pressure valve was installed downstream of the exhaust surge tank to control the exhaust pressure. The emissions analyzing system comprised of a set of California Analytical Instruments' 600 series analyzers which obtained the gas sample from the engine exhaust pipe through a heated line. The analyzers measured the concentrations of NO_x (detection limit: 5,000 ppm, resolution: 1 ppm), CH_4 (detection limit: 3,000 ppm, resolution: 1 ppm), carbon monoxide (CO) (detection limit: 5,000 ppm, resolution: 1 ppm), and CO_2 (detection limit: 20% vol., resolution: 0.01% vol.) in the exhaust gas.

An eddy current (EC) dynamometer was connected to the test engine in order to control the engine load according to the experimental requirements. An AVL angle encoder (365C) with a speed ranging from 50 to 20,000 RPM and a resolution of 0.01 CAD was used to determine the angular position of the crankshaft and engine speed. An AVL Digalog Test- mate system was used to interface with the engine electronic control unit to control the engine load and speed. An electric motor was used for motoring the engine to an engine speed of 500 revolution per minute (rpm), and subsequently the diesel fuel injection was initiated to fire the engine. A k-type thermocouple installed slightly down-stream of the exhaust valves measured the exhaust gas temperature. The exhaust gas temperature, lubricating oil pressure, exhaust gas oxygen concentration, exhaust gas emissions, flow rates of natural gas, diesel, and air, and cooling water temperature were recorded by a DAQ system based on LabVIEW platform over three minutes for each steady state test condition. A Kistler Piezo-Star 6125C pressure transducer continuously recorded cylinder pressure over 100 consecutive cycles at a sampling resolution of 0.2 crank angle degree (CAD). The cylinder pressure value was used to calculate the heat release rate (HRR) and other combustion characteristics.

2.2. Test Fuels

All tests were carried out using natural gas supplied by Enbridge Inc. and Canadian ultra-low sulfur diesel (ULSD). The lower heating value (LHV) of natural gas is 48.22 MJ/kg and that of diesel is 43.17 MJ/kg. The hydrogen to carbon (H/C) ratio of natural gas and diesel are 3.93 and 1.89, respectively. More properties of natural gas and diesel fuel can be found in Table 2.

Table 2. Fuel properties.

Property	Natural gas	Diesel
Density (kg/m^3)	0.711 (@ 15 °C and 1 atm)	814
Cetane number	-	44
LHV (MJ/kg)	48.22	43.17
H/C ratio	3.93	1.89
Composition (%vol.)	CH_4 : 95.17	-
	C_2H_6: 3.22	
	CO_2: 0.779	
	N_2: 0.743	
	Other component: 0.088	

137

138 *2.3. Experimental procedure and operating conditions*

139 In this study, a break mean effective pressure (BMEP) of 12.15 bar which is equivalent to 75% of full engine load
140 is selected for the experiments with a natural gas energy fraction of 50% and an engine speed of 910 rpm. The
141 selected engine load and speed is similar to the 13-mode EPA Supplemental Emissions Test (SET) of heavy-duty
142 engines. It is noted that during experiments, the control system adjusts the mass flow rates of diesel and natural gas
143 to maintain the engine load at BMEP of 12.15 bar. Since PM emissions are no longer a main issue in NDDF engines
144 and high-pressure diesel injection usually increases the peak pressure rise rate (PPRR) and NO_x emissions, a high-
145 pressure diesel injection is not necessary. On the other hand, very low injection pressure is not desirable in order to
146 ensure the atomization quality of diesel. Therefore, an appropriate diesel injection pressure of 525 bar was selected
147 in all tests of this investigation. Natural gas injection pressure and timing were maintained at 4.4 bar and -355° after
148 top dead center (ATDC), respectively. The intake pressure, intake temperature, and exhaust back pressure were fixed
149 at 1.80 bar, 40 °C, and 1.95 bar, respectively. To prevent engine damage, the maximum PPRR, cylinder pressure, and
150 exhaust gas temperature were maintained below 14 bar/CAD, 150 bar, and 600 °C, respectively. As shown in Table
151 3, the ratio of pre-injected diesel fuel was fixed at 25% for the pre-main-post and pre-main injection strategies. This
152 is due to the fact that increasing and decreasing the ratio of pre-injected diesel led to significant increase of the PPRR
153 and unreliable delivery of pre-injected diesel fuel, respectively, during the test.. To maintain stable combustion, the
154 coefficient of variation (COV) of indicated mean effective pressure (IMEP) was kept lower than 5%. In order to record
155 reliable exhaust emissions data, each test point reported in this paper represents the average of data collected over
156 a three minute duration at steady-state conditions, which was achieved when the exhaust gas temperature varied
157 by less than 1%.

158 Table 3 shows different diesel injection strategies used in the experiments. A schematic of diesel injection strategy
159 is also shown in Fig. 2. It is noted that SODI and EODI are defined as the start of diesel injection and end of diesel
160 injection, respectively. Diesel pulse width ratio (%PWR), which is calculated using Eq. (1), is defined as the ratio of
161 pulse width (PW) of each injection pulse (pre, main, or post) to the total diesel injection pulse width.

$$\%\mathrm{PWR} = \frac{\mathrm{PW_{D-pre,main,or\ post}}}{\mathrm{PW_{D-total}}} \quad (1)$$

162 The experiments started with a sweep of start of diesel injection (SODI) timing for diesel engine mode with single
163 diesel injection strategy (Test 1) in order to provide the baseline data for a comparative study. Then the engine was
164 switched to dual-fuel mode with 50% natural gas energy fraction under same engine load and speed conditions (i.e.,
165 BMEP = 12.15 bar and rpm = 910), and Test 2 started to investigate the effect of single diesel injection timing on the
166 NDDF engine performance. In order to do a comparison study, two diesel injection strategies of pre-main and main-
167 post were also examined in Tests 3 and 4, respectively. The diesel injection timing of the Tests 3 and 4 was optimized
168 to achieve the highest thermal efficiency and lowest GHG emissions. Our previous study found that operating a NDDF
169 engine with pre-main-post diesel injection strategy has the potential to further decrease the unburned methane
170 emissions under high load conditions [10]. However, the trade-off is lower indicated thermal efficiency (ITE) and
171 higher GHG emissions compared to that of single diesel injection strategy. In this paper, further effort is made to
172 improve the thermal efficiency and GHG emissions of the NDDF engine with pre-main-post diesel injection strategy
173 while reducing unburned methane and NO_x emissions compared to those with single diesel injection strategy.
174 Therefore, in Tests 5 to 7, the effect of pre-main-post diesel injection strategy on the NDDF engine was investigated.
175 In Test 5, a sweep of post diesel injection timing was conducted while the pre and main diesel injection timings were
176 fixed at -50 and -8 °ATDC, respectively. In Test 6, pre and post diesel injection timings were fixed at -50 and +30
177 °ATDC, respectively, while a sweep of the main diesel injection timing was conducted. In Tests 7, a sweep of the pre
178 diesel injection timing was carried out while the main and post diesel injection timings were fixed at -8 and +14
179 °ATDC, respectively.

Table 3: Diesel injection strategies.

Operating mode (injection strategy)	Diesel (kg/h)	NG (kg/h)	$SODI_{pre}$ (°ATDC)	$EODI_{pre}$ (°ATDC)	$SODI_{main}$ (°ATDC)	$EODI_{main}$ (°ATDC)	$SODI_{post}$ (°ATDC)	$EODI_{post}$ (°ATDC)	%PWR (pre/main/ post %)

		4.619				-14	+7.94			
		4.625				-16	+5.71			
		4.625				-18	+3.60			
Test 1	Diesel	4.649	-	-		-20	+2.80	-		-
	(Single)	4.731				-22	+1.34			
		4.759				-24	-2.72			
		4.842				-25	-3.72			
		2.311	2.087			-12	+0.90			
		2.279	2.061			-14	-1.27			
Test 2	Dual-fuel	2.257	2.035	-		-16	-3.33	-		-
	(Single)	2.701	2.027			-17	-4.22			
		2.264	2.026			-17.5	-4.76			
		2.307	2.063	-26	-21.97	-12	+0.07			
		2.298	2.054	-30	-25.95	-12	+0.14			
	Dual-fuel	2.310	2.065	-34	-29.95	-12	+0.14			
Test 3	(Pre-main	2.299	2.064	-38	-33.90	-12	+0.29	-		25/75
	with varying pre	2.297	2.058	-42	-37.85	-12	+0.43			
	injection timing)	2.285	2.053	-46	-41.86	-12	+0.41			
		2.283	2.041	-50	-45.88	-12	+0.33			
		2.327	2.103			-12	+0.37	+10	+14.12	
		2.343	2.100			-12	+0.40	+14	+18.13	
	Dual-fuel	2.351	2.114			-12	+0.30	+18	+22.10	
Test 4	(Main-post	2.354	2.113			-12	+0.34	+22	+26.11	
	with varying post	2.376	2.114	-		-12	+0.68	+26	+30.22	75/25
	injection timing)	2.352	2.117			-12	+0.71	+30	+34.23	
		2.375	2.119			-12	+0.58	+34	+38.19	
		2.380	2.126			-12	+0.61	+40	+44.20	
		2.322	2.076	-50	-44.91	-8	+2.17	+6	+11.08	
		2.358	2.085	-50	-44.79	-8	+2.41	+10	+15.20	
	Dual-fuel	2.365	2.131	-50	-44.73	-8	+2.53	+14	+19.26	
Test 5	(Pre-main-post 1	2.405	2.151	-50	-44.74	-8	+2.51	+18	+23.25	25/50/25
	with varying post	2.381	2.153	-50	-44.67	-8	+2.64	+22	+27.32	
	injection timing)	2.451	2.171	-50	-44.50	-8	+2.99	+26	+31.49	
		2.516	2.231	-50	-44.41	-8	+3.16	+30	+35.58	
		2.540	2.252	-50	-44.37	-8	+3.24	+40	+45.62	
	Dual-fuel	2.427	2.196	-50	-44.43	-10	+1.13	+30	+35.56	
Test 6	(Pre-main-post 2	2.474	2.220	-50	-44.44	-8	+3.10	+30	+35.55	25/50/25
	with varying main	2.471	2.215	-50	-44.49	-6	+5.00	+30	+35.50	
	injection timing)	2.546	2.272	-50	-44.46	-4	+7.06	+30	+35.53	
		2.321	2.101	-50	-44.76	-8	+2.46	+14	+19.23	
		2.307	2.053	-54	-48.76	-8	+2.47	+14	+19.23	
	Dual-fuel	2.298	2.052	-58	-52.81	-8	+2.37	+14	+19.18	
Test 7	(Pre-main-post 3	2.275	2.061	-62	-56.83	-8	+2.33	+14	+1916	25/50/25
	with varying pre	2.293	2.045	-66	-60.86	-8	+2.27	+14	+19.13	
	injection timing)	2.281	2.044	-70	-64.88	-8	+2.22	+14	+19.11	
		2.286	2.036	-75	-69.83	-8	+2.32	+14	+19.16	
		2.272	2.039	-80	-74.87	-8	+2.35	+14	+19.12	

180

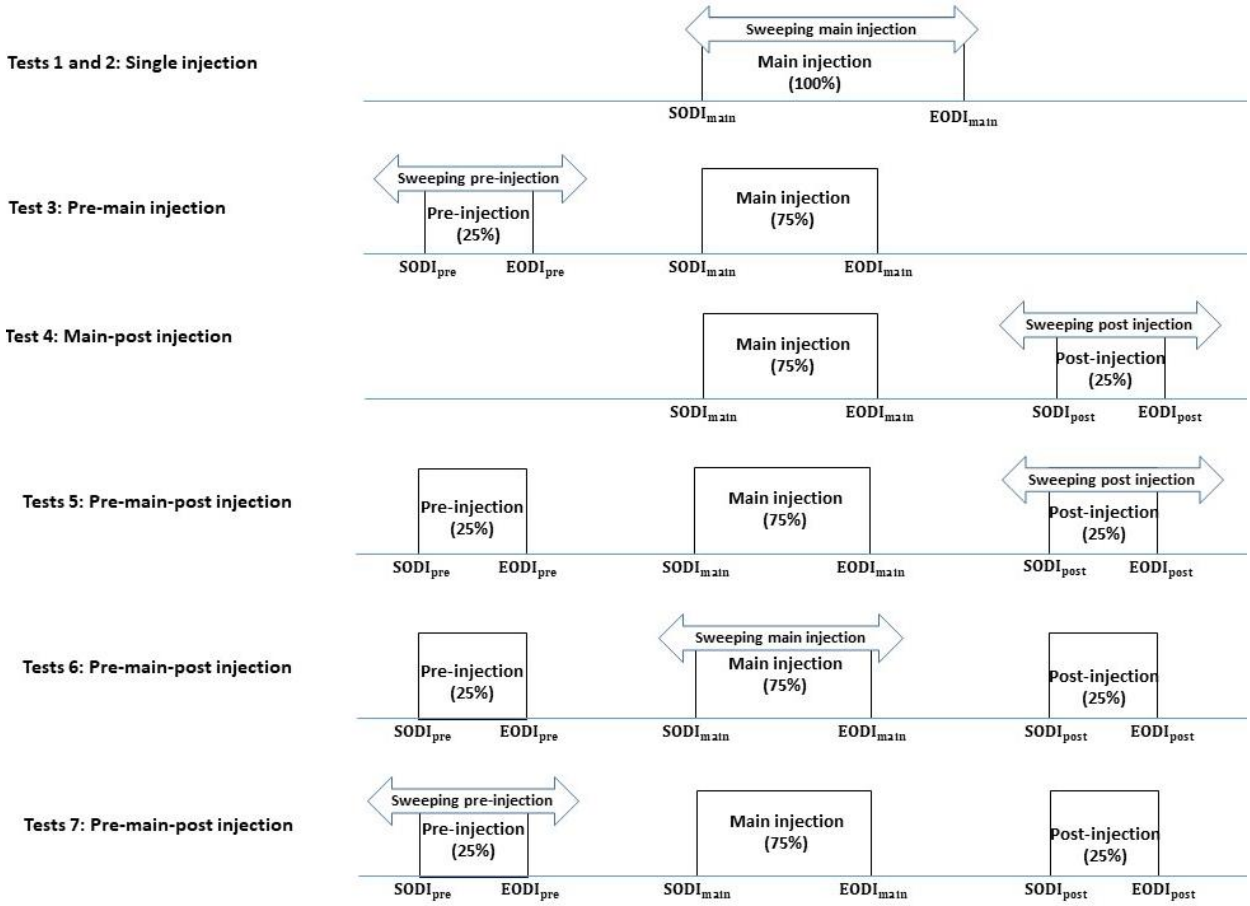

Fig. 2: Schematic of diesel injection strategies.

181

182 *2.4. Combustion characteristic metrics*

183 For each test point, the cylinder pressure data was used to calculate the net heat release rate (HRR) based on the
184 first law of thermodynamics using Eq. (2), where γ is the specific heat ratio, P is the cylinder pressure, V is the cylinder
185 volume, and θ is the engine crank angle.

$$\mathrm{HRR} = \frac{\gamma}{\gamma - 1} \mathrm{P} \frac{\mathrm{dV}}{\mathrm{d}\theta} + \frac{1}{\gamma - 1} \mathrm{V} \frac{\mathrm{dP}}{\mathrm{d}\theta} \qquad (2)$$

186 Indicated thermal efficiency (ITE) was calculated using Eq. (3) where $\mathrm{P_{ind}}$ is indicated power, $\dot{\mathrm{m}}_{\mathrm{NG}}$ and $\dot{\mathrm{m}}_{\mathrm{D}}$ are the
187 mass flow rate of natural gas and diesel, respectively, and $\mathrm{LHV_{NG}}$ and $\mathrm{LHV_{D}}$ are the lower heating value of natural
188 gas and diesel, respectively.

$$\mathrm{ITE} = \frac{\mathrm{P_{ind}}}{\dot{m}_{\mathrm{D}} \times \mathrm{LHV_D} + \dot{m}_{\mathrm{NG}} \times \mathrm{LHV_{NG}}} \quad (3)$$

The natural gas energy fraction (%NG), Eq. 4, is defined as the fraction of energy from natural gas in the total energy input to the engine.

$$\%\mathrm{NG} = \frac{\dot{m}_{\mathrm{NG}} \times \mathrm{LHV_{NG}}}{\dot{m}_{\mathrm{D}} \times \mathrm{LHV_D} + \dot{m}_{\mathrm{NG}} \times \mathrm{LHV_{NG}}} \quad (4)$$

Combustion phasing (i.e., CA50) is determined as the crank angle where 50% of the total heat energy from the fuel is released. The zero-crossing point of heat release curve when heat release rate starts to increase is defined as start of combustion (SOC). The pressure rise rate is calculated from the pressure profiles using Eq. (5), where P represents the discrete pressure signal and $\Delta\theta$ is 0.2 CAD since the cylinder pressure data is collected at an interval of 0.2 CAD.

$$\left(\frac{\mathrm{dP}}{\mathrm{d}\theta}\right)_{\mathrm{i}} = \frac{\mathrm{P_{i+1}} - \mathrm{P_i}}{\Delta\theta} \quad (5)$$

3. Numerical approach

A three-dimensional CFD simulation was conducted using a commercial software, CONVERGE (version 3.0) [41], to understand the mechanisms of the experimental observations. The details of numerical modeling can be found in our previous studies [10,36,42–44] and a brief summary of the numerical method and important models are presented in this section. The conservation equations of mass, momentum, species, and energy were discretized by a second-order scheme in space and a first-order scheme in time. The CFD code calculated the transport equations and a transient chemistry solver, SAGE [41], calculated the reaction rate of each elementary reaction. Diesel and natural gas were represented by n-heptane and methane, respectively, using a reduced reaction mechanism consisting of 76 species and 464 reactions [45]. An Eulerian-Lagrangian Discrete Droplet Model (DDM) was used to model the spray [41]. The Kelvin-Helmholtz Rayleigh-Taylor (KH-RT) model was adopted to model diesel droplet atomization and breakup [46]. The collision of diesel spray droplets was simulated by O'Rourke model [47]. Adaptive mesh refinement (AMR) was used to efficiently resolve details in the regions of the higher species concentration

gradients and the turbulent flame front [41]. The maximum size of computational cell was set at 2.0 mm. However, a very fine grid resolution was needed to capture the subgrid-scale effects on flame propagation. AMR allowed the automatic reduction of the computational cell size to 0.25 mm in order to capture the turbulent flame front (Fig. 3).

A closed cycle simulation from intake valve closing (IVC) to exhaust valve opening (EVO) was carried out in this study. As shown in Table 1, since the diesel injector had six equally spaced nozzle's orifices, a 1/6th section of the combustion chamber was simulated as a representative volume of the entire chamber. Premixed natural gas – air mixture was assumed to be homogeneous at the beginning of the simulation since a port fuel injection of natural gas was used in the experiments. The cylinder charge temperature at the start of simulation was calculated by 1-D simulation in GT-POWER. This temperature was kept at 360 K for all simulated cases since the engine load and speed were maintained at BMEP = 12.15 bar and rpm = 910, respectively, during the experiments. As mentioned in section 2.3, the intake manifold pressure was maintained at 1.80 bar in all tests. However, in order to reproduce the trapped mass and experimental cylinder pressure during the compression stroke the cylinder charge pressure at the start of simulation was slightly adjusted (1.80 ± 0.02 bar).

According to the study of Wijeyakulasuriya et al. [48], the combustion process and emissions become very sensitive to wall boundary temperatures when the combustion starts from the outer periphery or near the liner and then propagates inward. Therefore, estimation of wall boundary temperature is a crucial part of this simulation study, especially for pre-main and pre-main-post diesel injection strategies where part of the diesel fuel is injected at a very advanced timing during the compression stroke and the combustion starts from near the cylinder liner and piston squish regions. The detailed explanation of boundary temperature estimation was presented in our recent study [10] and a brief description is given in this section. It was shown in our previous study [10] that post-injection strategies increase the exhaust gas temperature since part of diesel fuel is burnt very late in the expansion stroke. This increases the subsequent cycle boundary wall temperatures due to the high temperature of residual gas in the combustion chamber. To take this into account in the closed cycle simulation and to precisely predict the initial wall boundary temperature, three consecutive closed cycle simulations were performed for each case. After completion of the first simulation, the average charge temperatures near the wall were calculated and applied for the second simulation, and those from the second simulation were applied to the third simulation. Finally, an appropriate value

234 of boundary temperature was established by comparing the predicted start of combustion, EVO temperature, and
235 unburned methane emissions with their experimental counterparts [10].

236 In order to verify the reliability of the developed CFD model, four different diesel injection strategies (i.e., single,
237 pre-main, main-post, and pre-main-post) are selected to compare the measured and calculated cylinder pressure
238 and heat release rate of the NDDF engine. As shown in Fig. 4, the calculated cylinder pressure and heat release rate
239 are in good agreement with the experimental results, suggesting that the combustion process is well reproduced by
240 the CFD model. The calculated results of thermal efficiency, combustion phasing, start of combustion, PPRR, and
241 unburned methane, NO_x, and GHG emissions of some selected cases of pre-main-post diesel injection strategy will
242 be presented and compared with experimental results in section 4. More validation of single, pre-main, and main-
243 post diesel injection strategies can be also found in our previous study [10]. It is noted that the ISCH4 and ISCO2
244 emissions were under-predicted (Figs. 9a and b). This is mainly due to the use of reduced methane/n-heptane
245 chemical mechanism in CFD simulations. Moreover, there is a discrepancy between calculated and measured
246 thermal efficiency as shown in Fig. 9c. The calculated cylinder pressure is higher than measured one during the
247 expansion stroke (Fig. 4) which leads to over-prediction in thermal efficiency. This could be due to the deficiencies
248 in adopted wall heat transfer model and the assumption of constant boundary wall temperature.

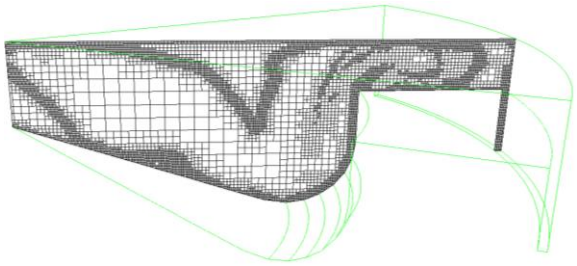

Fig. 3: Adaptive mesh refinement in flame front during the flame propagation stage.

249

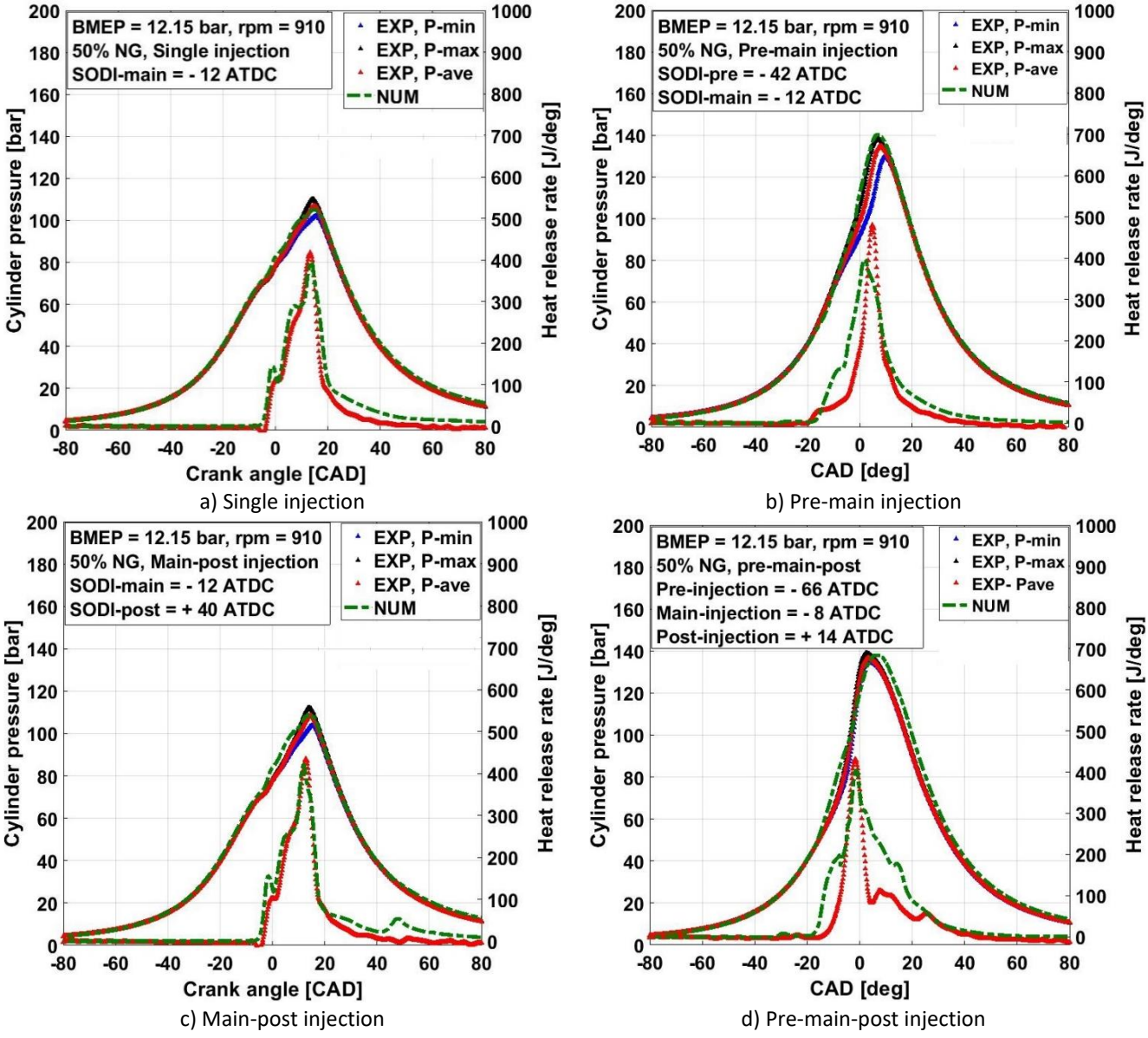

Fig. 4: Measured and calculated cylinder pressure and HRR of single, pre-main, main-post, and pre-main-post diesel injection strategies.

4. Results and discussion

In this section, the effect of pre-main-post diesel injection strategies on combustion characteristics (i.e., cylinder pressure, HRR, exhaust temperature, start of combustion (SOC), combustion phasing, PPRR, and thermal efficiency) and emissions (i.e., CH_4, NO_x, and GHG) of the NDDF engine is investigated at 50% natural gas energy fraction. The experimental results of pre-main-post injection strategy are also compared with single, pre-main, and main-post diesel injection strategies. The focus is on the optimization of combustion phasing and thermal efficiency of pre-

main-post injection strategy while maintaining its lower unburned methane emissions compared to single diesel injection strategy. Numerical simulation results are presented for selected cases in order to improve the understanding of the fundamental mechanisms observed in the experiments.

Figures 5a, b, and c show the effects of post, main, and pre diesel injection timings, respectively, on cylinder pressure and HRR of the investigated NDDF engine with pre-main-post diesel injection strategy. Only the effect of selected diesel injection timings on cylinder pressure and HRR is displayed in these figures. The effects of single, pre-main, and main-post diesel injection strategies on cylinder pressure and HRR of the NDDF engine have been investigated and discussed in our previous study [10], and therefore are not shown in this section. Figure 6 displays the effect of pre, main, and post diesel injection timings on exhaust temperature and SOC for various injection strategies. It can be seen from Figs. 5 and 6b that the SOC occurs before the main diesel injection timing for all examined pre-main-post diesel injection strategies, implying that the premixed mixture of pre-injected diesel and natural gas – air is ignited before the main diesel injection timing. This is also confirmed by Hydroxyl (OH) radical distribution contours for a selected case of SODI-pre, main, and post = - 62, - 8, and +14 °ATDC, respectively, in Fig. 7. It is observed that the OH radical initially appears in the piston squish area at an engine crank angle of -15.69 °ATDC that is 7.69 °CAD before the main diesel injection timing (SODI-main = - 8 °ATDC). The second zone of OH radical is also detected two crank angle degree later in the piston crevice region. At an engine crank angle of CAD = -10.69 °ATDC, the two flame kernels merge and propagate towards the cylinder center.

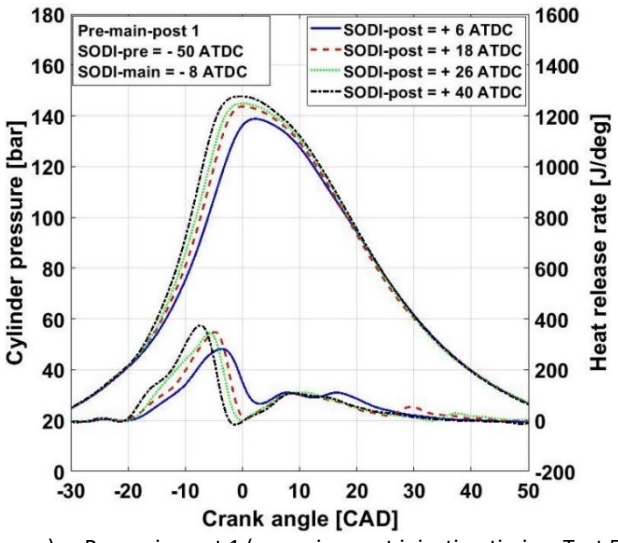

a) Pre-main-post 1 (sweeping post injection timing, Test 5)

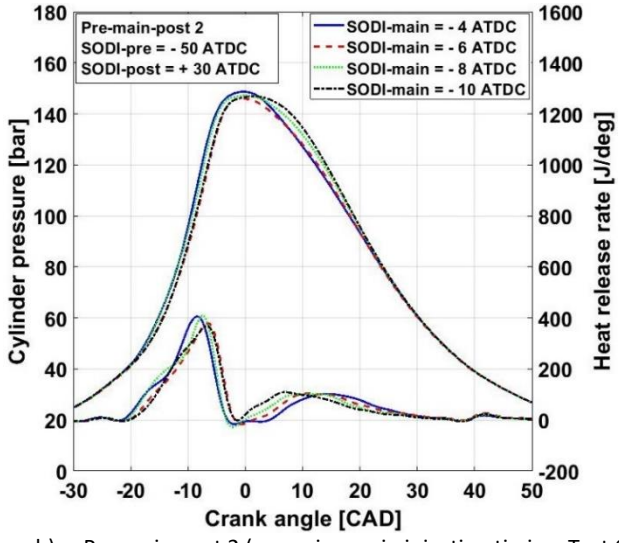

b) Pre-main-post 2 (sweeping main injection timing, Test 6)

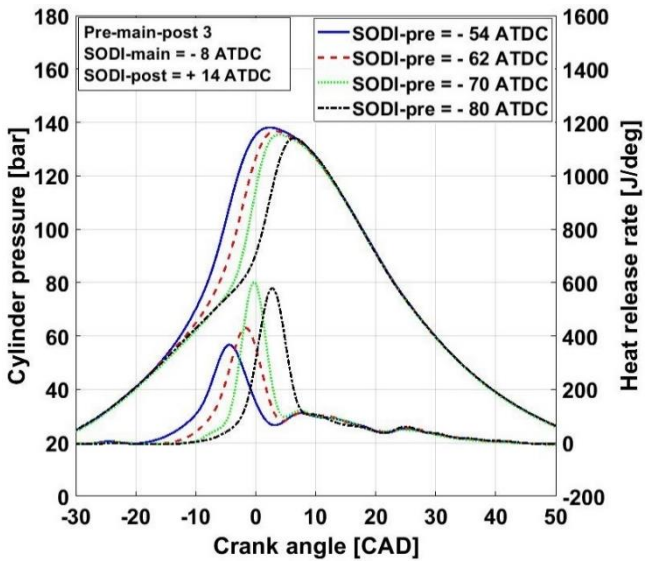

c) Pre-main-post 3 (sweeping pre injection timing Test 7)

Fig. 5: Measured cylinder pressure and HRR of NDDF engine with different pre-main-post diesel injection strategies.

273

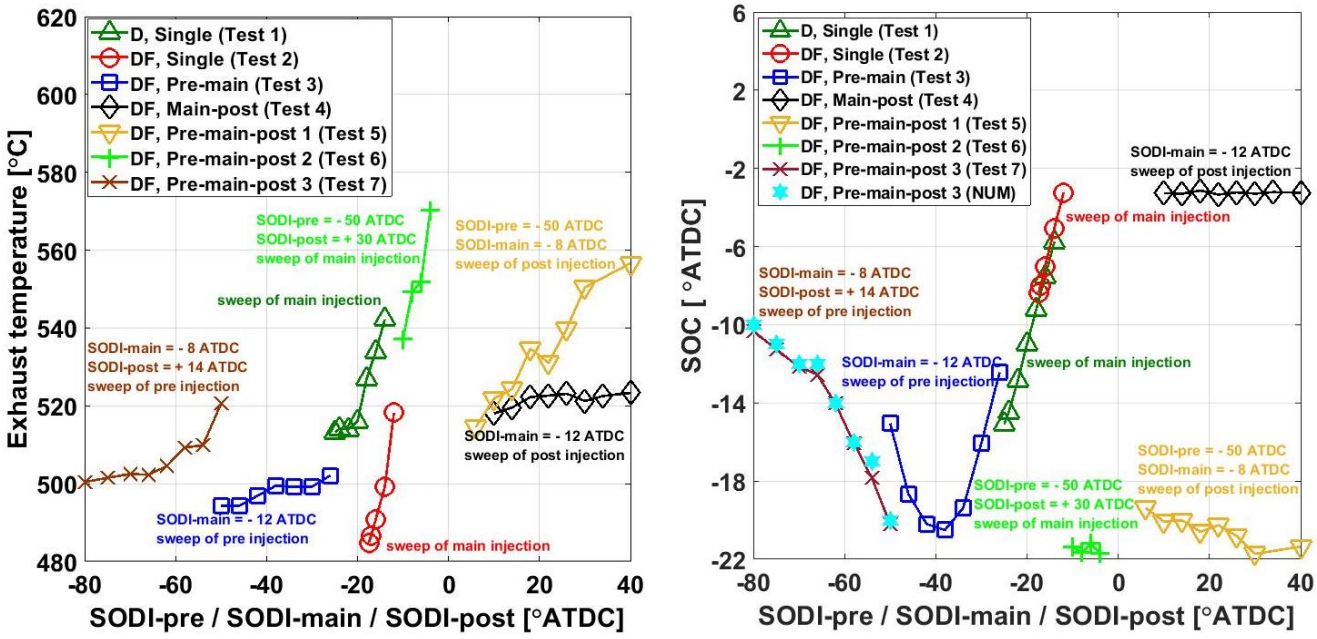

a) Exhaust gas temperature b) Start of combustion

Fig. 6: Exhaust gas temperature and SOC of NDDF engine with different diesel injection strategies.

274

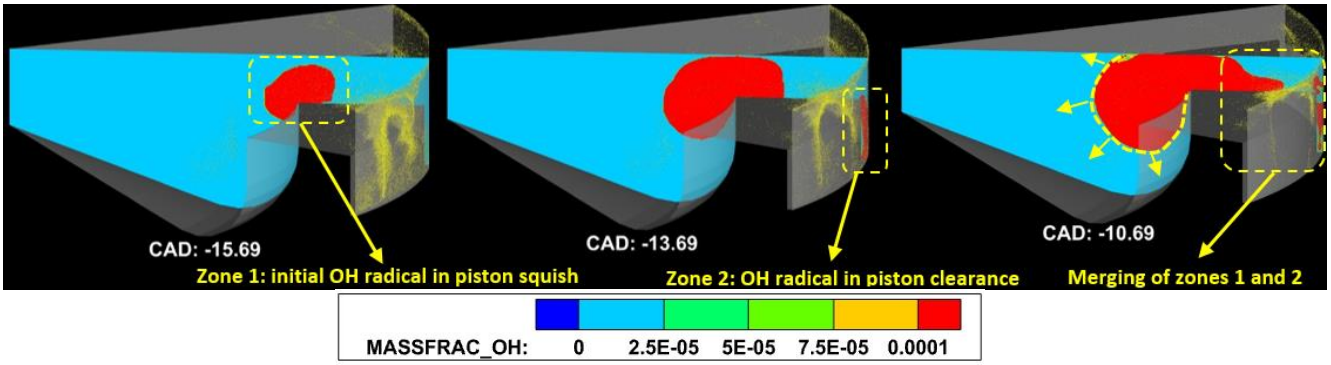

Fig. 7: OH radical distribution of NDDF engine with pre-main-post diesel injection strategy with SODI-pre, main, and post = - 62, - 8, and + 14 °ATDC at 50% natural gas energy fraction.

As shown in Figs. 5a and 6b (Test 5), retarding post diesel injection timing advances the start of combustion of the NDDF engine with pre-main-post diesel injection strategy. This is mainly due to the exhaust gas temperature increase with retarding post diesel injection timing, as shown in Fig. 6a, which increases the wall and cylinder charge temperature of the subsequent cycle and thus advances the SOC. As shown in Figs. 6a and b, for Test 5, retarding post diesel injection timing from +6 to +40 °ATDC increases the exhaust gas temperature from 514.53 to 556.62 °C and advances the start of combustion from -19.3 to -21.2 °ATDC. The reason behind this phenomenon was explained in our previous study along with cylinder charge temperature and local equivalence ratio contours [10]. Due to the same reasons, retarding main diesel injection timing (Test 6) also advances the SOC.

As mentioned above, the start of combustion occurs before the main diesel injection timing for all pre-main-post diesel injection strategies (see Fig. 6b, Tests 5 and 6). This suggests that the cylinder charge temperature and the timing of pre injected diesel affect the stratification of pre-injected diesel and natural gas – air mixture and control the start of combustion. In order to prove this, the effect of sweeping pre diesel injection timing on cylinder pressure and HRR of the NDDF engine is examined in Fig. 5c (Test 7). It is observed that sweeping pre diesel injection timing has more significant effect on SOC compared to sweeping main and post diesel injection timings (Tests 5 and 6, Figs. 5a and b). This is more clearly shown in Fig. 6b. Similar to sweeping main and post diesel injection timing (Tests 5 and 6), retarding the pre diesel injection timing also increases the exhaust gas temperature (Fig. 6a). The change in the pre diesel injection timing modifies the stratification of pre injected diesel and natural gas – air mixtures and therefore the local equivalence ratio inside the combustion chamber before start of combustion. To further elucidate this, the cylinder charge temperature and local equivalence ratio contours with two different pre diesel injection

timings of -80 and -50 °ATDC and fixed main and post diesel injection timings are shown in Fig. 8. It is noted that the frame contours in Fig. 8 were selected at an engine crank angle before the start of combustion (i.e., CAD = - 23 .68 °ATDC) to compare the cylinder charge temperature and the local equivalence ratio. It can be seen that the average charge temperature in piston squish regions for the pre-main-post injection strategy with pre diesel injection timing of -50 °ATDC (T-ave-squish = 956.21 °C) is higher than that of -80 °ATDC (T-ave-squish = 912.08 °C). This is due to the higher exhaust gas temperature with pre diesel injection timing of -50 °ATDC, which increases the wall and cylinder charge temperature of the subsequent cycle. Moreover, the local equivalence ratio contours show that the pre injected diesel for both pre injection timings of -50 and -80 °ATDC targets the piston squish and crevice regions. However, retarded pre diesel injection timing of -50 °ATDC provides a higher local equivalence ratio regions in the piston squish and crevice regions (Fig. 8). Therefore, the higher cylinder charge temperature at piston squish regions along with higher local equivalence ratio of diesel injection strategy with pre diesel injection timing of -50 °ATDC results in more advanced SOC compared to that of -80 °ATDC.

From the above discussion, it can be inferred that two parameters affect the SOC when retarding the pre diesel injection timing in pre-main-post injection 3 test. The first one is the thermal effect of exhaust temperature when retarding diesel injection timing, which is also found in pre-main-post 1 and 2 tests where the SOC also slightly advances (in the range of 1 to 2 CAD) when retarding post and main diesel injection timings. The second one is fuel stratification of natural gas – air – pre injected diesel and it seems more significant than the thermal effect. This is because retarding pre diesel injection timing increases the exhaust temperature by only 20 °C that is even smaller than the exhaust temperature increase in pre-main-post 1 and 2 tests (in the range of 30 to 40 °C) when retarding post and main diesel injection timings. Therefore, it is concluded that the thermal effect of retarding pre diesel injection timing could advance the SOC by 1 to 2 CAD, but the SOC advancement may be mainly a result of the fuel stratification effect of the premixed mixture of pre injected diesel and natural gas – air.

As mentioned above, the goal of this paper is to retard the combustion phasing (or SOC) of the NDDF engine with pre-main-post diesel injection strategy to a more optimized crank angle. Sweeping pre-diesel injection timing gives more controllability of combustion phasing (start of combustion) than sweeping main and post diesel injection timings. It is found that a stratified premixed mixture of pre injected diesel – natural gas – air (e.g. SODI-pre = -50

°ATDC) leads to overly advanced combustion phasing (or start of combustion) which decreases the thermal efficiency of the NDDF engine with pre-main-post diesel injection strategy. However, a more homogenous premixed mixture of pre injected diesel – natural gas – air (e.g. SODI-pre = -80 °ATDC) retards the combustion phasing and improves the thermal efficiency of the NDDF engine. More details will be discussed in Figs. 9c and d.

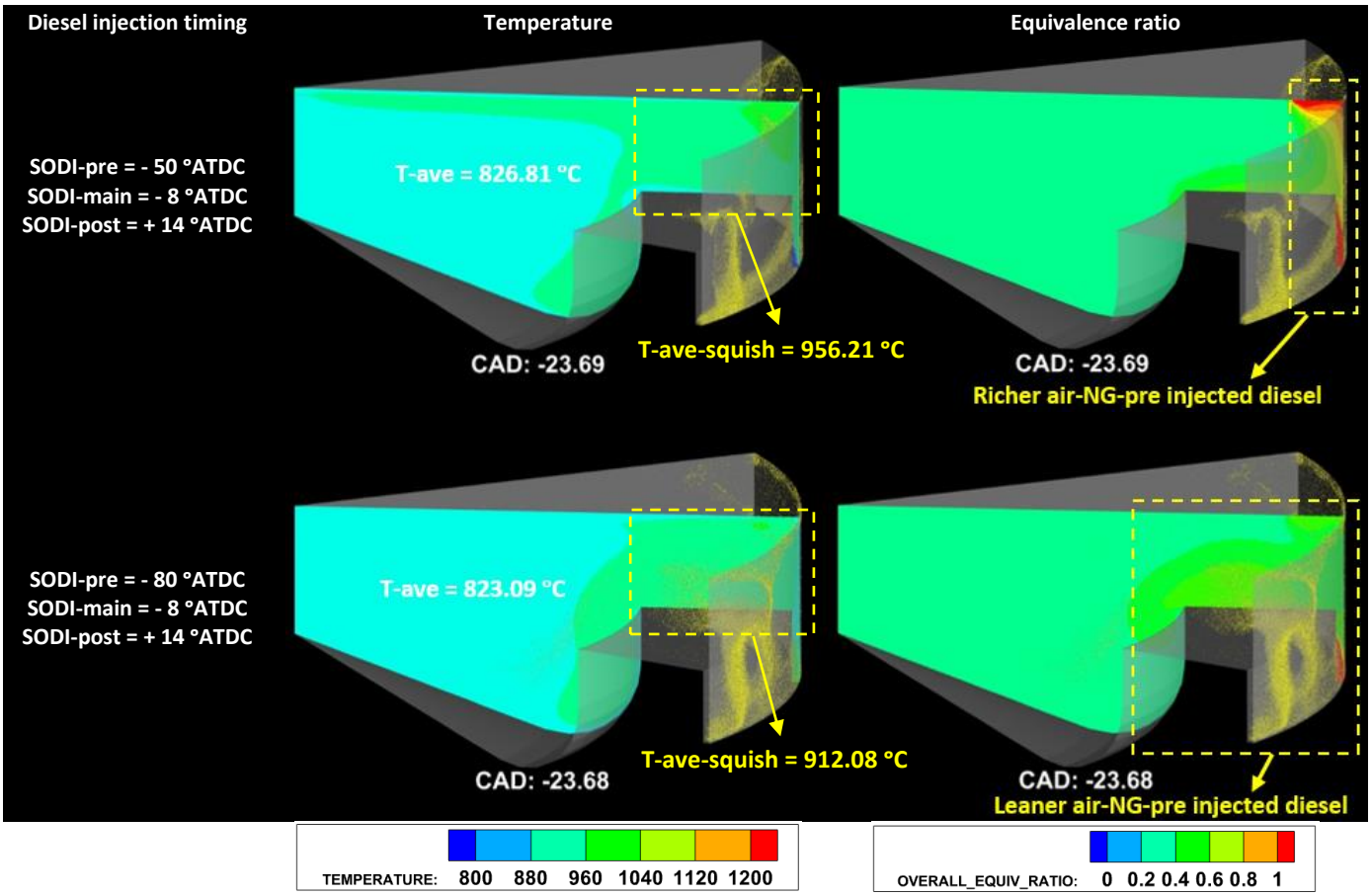

Fig. 8: Cylinder temperature and local equivalence ratio contours of NDDF engine with two different pre diesel injection timing of -80 and -50 °ATDC and fixed main and post injection timings at SOC.

Figures 9a-d display the CO_2 equivalent (or GHG) and unburned methane emissions, indicated thermal efficiency (ITE), and combustion phasing for different diesel injection strategies at 50% natural gas energy fraction. The results of Test 6 (pre-main-post 2) are not shown here since sweeping main diesel injection timing of pre-main-post injection strategy has little effect on the results. In this study, the equivalent CO_2 emission is calculated using Eq. (6) according to EPA's GHG emissions-Phase (II) [39].

$$\text{Equivalent ISCO}_2 = \text{ISCO}_2 + 34 \times \text{ISCH}_4 \quad (6)$$

It is observed from Figs. 9a and c (Test 1) that the diesel engine mode with single injection achieves the lowest GHG emissions of 650.11 g/kW.h and the highest ITE of 40.48% at the diesel injection timing of -22 °ATDC. The NDDF engine mode with single diesel injection strategy (Test 2) obtains higher ITE and emits lower GHG emissions compared to its counterpart diesel engine mode. As shown in Figs. 9a and c, advancing single diesel injection timing from -12 to -16 °ATDC improves both GHG emissions and ITE of the NDDF engine. The lowest GHG emissions and highest ITE are 609.77 g/kW.h and 40.72%, respectively, which occur at the single diesel injection timing of -16 °ATDC (Test 2). It is noted that the unburned methane emissions monotonically increase with advancing the single diesel injection timing, since the increase in cylinder pressure causes more natural gas-air mixture to be trapped in the crevice and boundary zones [42]. Therefore, the decrease of GHG emissions with advancing of the single diesel injection timing from -12 to -16 °ATDC is due to the improvement in ITE. The emitted unburned methane emissions at the optimum point of ITE and GHG emissions is 1.12 g/kW.h. Further advancing diesel injection timing to -17.5 °ATDC increases the GHG emissions and decreases the ITE. These are due to the increase of unburned methane emissions (Fig. 9b) and overly advanced combustion phasing (Fig. 9d).

Advancing pre diesel injection timing improves both GHG emissions and ITE of the NDDF engine with pre-main diesel injection strategy (Test 3), as shown in Figs. 9a and c. However, advancing pre diesel injection timing increases the unburned methane emissions of the NDDF engine using pre-main diesel injection strategy (Test 3). The lowest GHG emissions of 617.94 g/kW.h and the highest thermal efficiency of 40.4% of the NDDF engine with pre-main diesel injection strategy are obtained at the pre diesel injection timing of -50 °ATDC. The emitted unburned methane emissions at the optimum point of GHG emissions in the pre-main injection strategy is 1.25 g/kW.h, which is higher than that of the single diesel injection strategy.

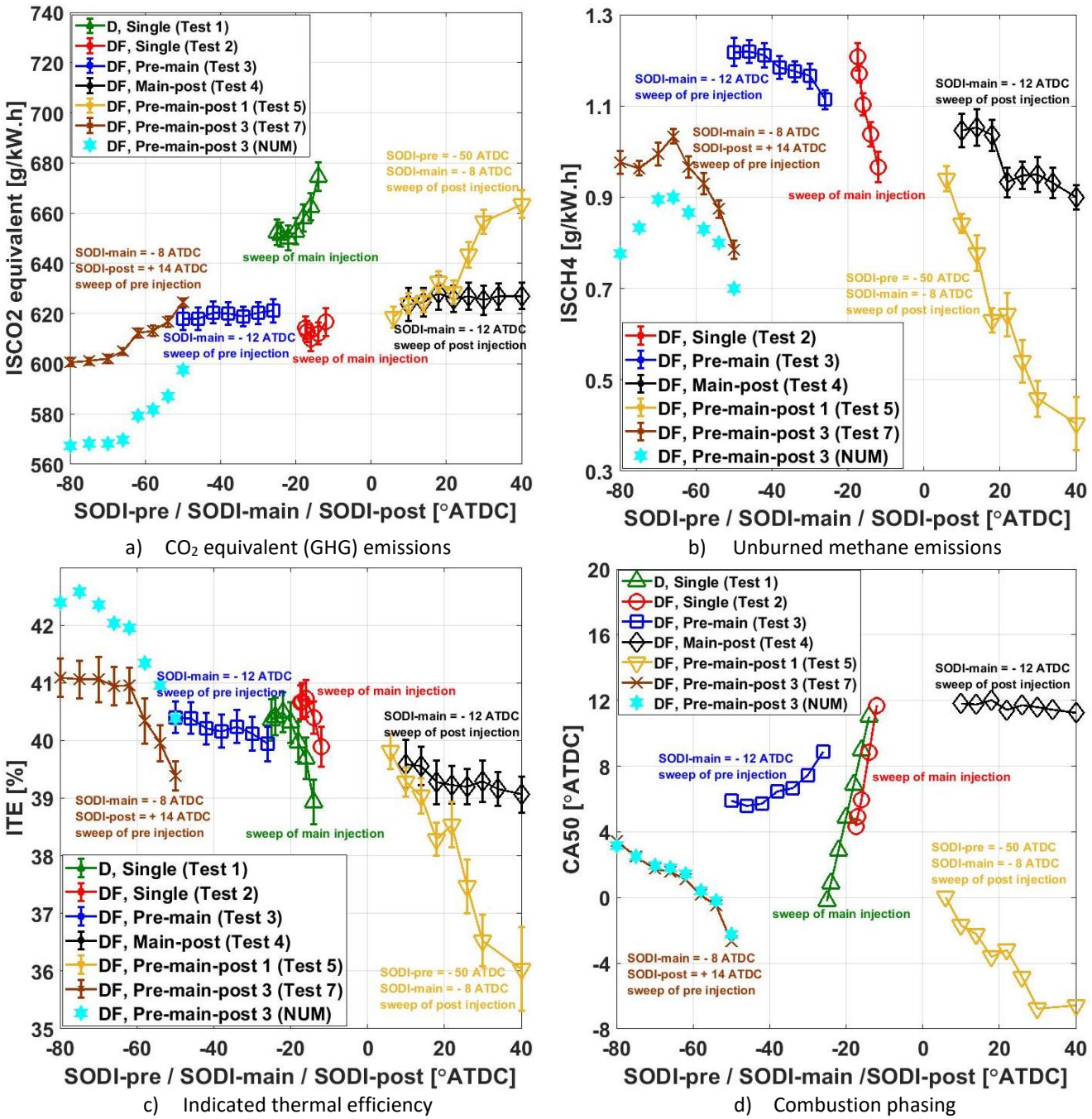

a) CO_2 equivalent (GHG) emissions

b) Unburned methane emissions

c) Indicated thermal efficiency

d) Combustion phasing

Fig. 9: GHG and unburned methane emissions, ITE, and combustion phasing of NDDF engine with different diesel injection strategies.

It can be observed from Fig. 9b that retarding the post diesel injection timing decreases the unburned methane emissions of the NDDF engine with both main-post (Test 4) and pre-main-post 1 (Test 5). The reduction is more significant when using pre-main-post. This is because pre diesel injection burns most of the trapped unburned methane in the crevice regions at the beginning of the combustion, and post diesel injection increases the cylinder charge temperature in the late expansion stroke and pushes the remaining unburned gas in the crevice regions into

the second-stage of combustion [10]. However, as shown in Fig. 9a, retarding post diesel injection timing increases the GHG emissions of the NDDF engine, especially for the pre-main-post 1 test (Test 5). This is mainly caused by the overly advanced combustion phasing (Fig. 9d), which subsequently causes deterioration in thermal efficiency (Fig. 9c) as post diesel injection timing is retarded. Therefore, if the combustion phasing of the NDDF engine can be retarded while maintaining the low unburned methane emissions feature of the pre-main-post diesel injection strategy, it may be possible to further reduce GHG emissions. To reach this goal, the pre-diesel injection timing is further advanced in the pre-main-post 3 test (Test 7) compared to that in pre-main-post injection 1 test (Test 5). It is observed from Fig. 9d that the combustion phasing is retarded, and therefore ITE and GHG emissions are further improved as the pre-diesel injection timing is advanced in the pre-main-post diesel injection strategy (Test 7). The lowest GHG emissions and the highest thermal efficiency of the NDDF engine in pre-main-post 3 test are 600.68 g/kW.h and 41.09%, respectively, which are achieved at an advanced pre-diesel injection timing of -80 °ATDC. Moreover, the emitted unburned methane emissions at this optimum point of GHG emissions is 0.97 g/kW.h. This is about 13.4% reduction in unburned methane emissions compared to optimum point of the single diesel injection strategy.

Figure 10 shows the effect of different diesel injection strategies on PPRR of the NDDF engine at 50% natural gas energy fraction. It can be observed that advancing diesel injection timing significantly increases the PPRR of the NDDF engine with single diesel injection strategy (Test 2), in which the PPRR reaches 10.88 bar/CAD at the optimum point of GHG emissions (i.e., SODI = -16 °ATDC). Double and triple diesel injection strategies allow wider ranges of diesel injection timing while keeping the maximum PPRR well below the engine limit. For example, advancing pre-diesel injection timing in pre-main-post 3 test (Test 7) from -50 to -70 °ATDC increases the maximum PPRR of the NDDF engine from 8.37 to 10.31 bar/CAD, but the PPRR starts to decrease with further advancement of the pre-diesel injection timing. The PPRR of 9.11 bar/CAD is achieved at the optimum point of GHG emissions of the NDDF engine with pre-main-post 3 test (i.e., SODI-pre = -80 °ATDC). This is about 16.2% reduction of PPRR compared to the optimum point of single diesel injection strategy.

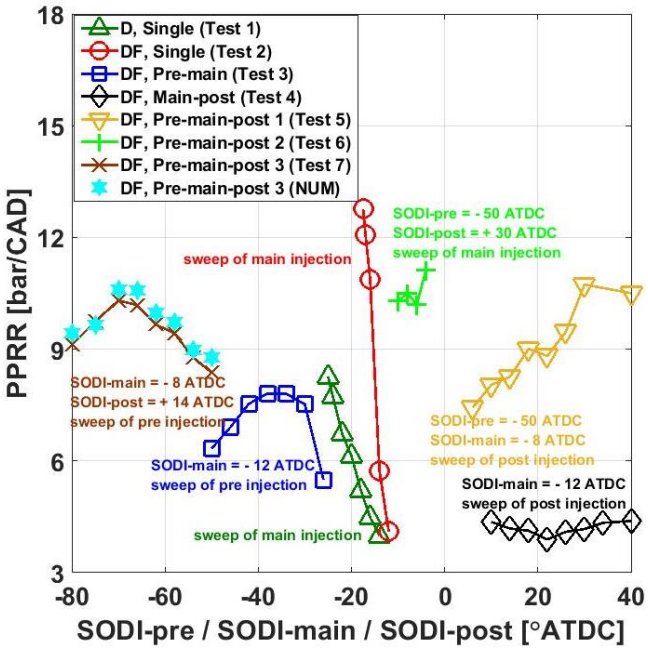

Fig. 10: Peak pressure rise rate of NDDF engine with different diesel injection strategies at 50% natural gas energy fraction.

Figure 11 displays the effect of different diesel injection strategies on NO_x emissions and NO_x – GHG trade off of the NDDF engine at 50% natural gas energy fraction. The results of diesel engine mode with single diesel injection strategy are also added for the sake of comparison. It can be observed from Fig. 11a that the NDDF engine with single diesel injection strategy (Test 2) produces higher NO_x emissions compared to that of diesel engine mode (Test 1) at similar single diesel injection timing. This is mainly because of the faster burning rate of natural gas – air – diesel mixtures in NDDF engine mode than that of air – diesel mixtures in diesel engine mode once it is being ignited. This faster burning rate advances the SOC (Fig. 6b) and CA50 (Fig. 9d) and increases the combustion temperature and therefore the NO_x emissions of the NDDF engine mode compared to the diesel engine mode. However, the emitted NO_x emission of the diesel engine mode at the optimum point of GHG emissions (Fig. 11b, SODI = - 22 ATDC, Test 1) is 9.21 g/kW.h, while this value is 6.93 g/kW.h for the NDDF engine with single diesel injection strategy (Fig. 11b, SODI = -16 °ATDC, Test 2).

The injection of part of diesel before the main injection timing in pre-main injection strategy (Test 3) decreases the NO_x emissions of the NDDF engine compared to that at the optimum GHG point of single diesel injection strategy. The NDDF engine with pre-main diesel injection strategy produces 5.78 g/kW.h NO_x emissions at the optimum point

of GHG emissions (Fig. 11b, SODI-pre = -50 °ATDC, Test 3). However, as shown in Fig. 11b, the value of GHG emissions at this point is higher than that of single diesel injection strategy.

Retarding post diesel injection timing in pre-main-post 1 test (Test 5) significantly increases NO_x and GHG emissions (Fig. 11b) of the NDDF engine. The NDDF engine emits 5.06 g/kW.h NO_x emissions in pre-main-post 1 test (Test 5) at the optimum point of GHG emissions (SODI-post = + 6 °ATDC), which is 618.61 g/kW.h and higher than that of single diesel injection strategy. As shown in Fig. 11b, the NDDF engine can obtain the lowest NO_x and GHG emissions simultaneously in pre-main-post 3 test (Test 7), which are 4.01 g/kW.h and 600.68 g/kW.h, respectively, at SODI-pre = - 80 °ATDC. These are almost 42% and 1.5% reductions, respectively, in NO_x and GHG emissions compared to those at the optimum point of GHG emissions in single diesel injection strategy.

Hence, the NDDF engine can achieve comparable or even better thermal efficiency and GHG emissions while reducing unburned methane and NO_x emissions by 13.4% and 42%, respectively and PPRR by 16.2% in the pre-main-post injection 3 test (Test 7) compared to those at the optimum point of the NDDF engine with the single diesel injection strategy.

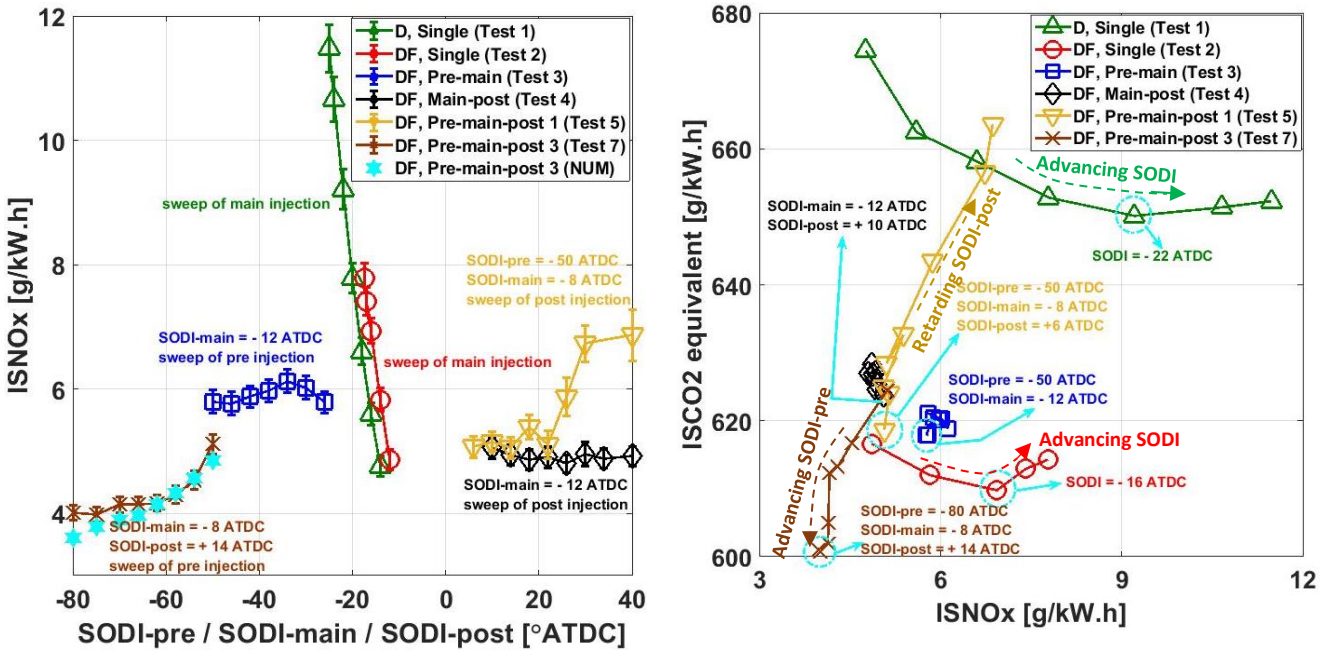

a) ISNOx b) NOx – GHG trade off

Fig. 11: NO_x emissions and NO_x – GHG trade off of NDDF engine with different diesel injection strategies.

5. Conclusions

The effect of pre-main-post diesel injection strategy on combustion performance and emissions of a NDDF engine at 50% natural gas energy fraction and high load conditions has been investigated with focus on further improving engine efficiency and GHG emissions.

The results reveal that the change in pre-diesel injection timing gives more controllability on the combustion phasing (start of combustion) than that in main and post diesel injection timings for pre-main-post injection strategy, since it modifies both fuel stratification and thermal conditions inside the combustion chamber before the start of combustion. It is found that a stratified premixed mixture of pre injected diesel – natural gas – air (e.g. SODI-pre = -50 °ATDC) leads to overly advanced combustion phasing which decreases the thermal efficiency of the NDDF engine with pre-main-post diesel injection strategy. However, a more homogenous premixed mixture of pre injected diesel – natural gas – air (e.g. SODI-pre = -80 °ATDC) retards the combustion phasing which allowed further improvement of the indicated thermal efficiency and GHG emissions of the NDDF engine while maintaining the low unburned methane emissions feature of the pre-main-post diesel injection strategy. The lowest GHG emissions of 600.68 g/kW.h and the highest ITE of 41.09% were achieved in pre-main-post diesel injection strategy using very advanced pre diesel injection timing of -80 °ATDC. This is slightly better than the optimum point of the NDDF engine when using single diesel injection strategy (GHG = 609.77 g/kW.h and ITE = 40.72%). The emitted unburned methane emissions at this optimum point of GHG emissions was reduced by 13.4% compared that of the NDDF engine with single diesel injection strategy. Moreover, using pre-main-post diesel injection strategy decreased the PPRR and NO_x emissions by 16.2% and 42%, respectively, compared to the optimum point of GHG emissions of the single diesel injection strategy.

Acknowledgement

Funding of the experimental and numerical works was provided by Natural Resources Canada through the PERD Energy End Use Program and National Research Council Canada (NRC) through the internal Advanced Clean Energy Program. The numerical simulation was supported by CONVERGENT Science Inc.

Nomenclature

AMR	Adaptive Mesh Refinement
ATDC	After Top Dead Center
BMEP	Brake Mean Effective pressure
CA50	Crank Angle of 50% Cumulative Heat Release
CAD	Crank Angle Degree
CAI	California Analytical Instruments
CFD	Computational Fluid Dynamic
CH_4	Methane
CI	Compression Ignition
CO	Carbon Monoxide
CO_2	Carbon Dioxide
COV	Coefficient Of Variation
DAQ	Data Acquisition
DDM	Discrete Droplet Model
DI	Direct Injection
EC	Eddy Current
EODI	End Of Diesel Injection
EPA	Environmental Protection Agency
EVO	Exhaust Valve Opening
GHG	GreenHouse Gas
HRR	Heat Release Rate
ICE	Internal Combustion Engine
IMEP	Indicated Mean Effective Pressure
$ISCH_4$	Indicated Specific CH_4
$ISCO_2$	Indicated Specific CO_2
$ISNO_x$	Indicated Specific NO_x
ITE	Indicated Thermal Efficiency
IVC	Intake Valve Closing
KH-RT	Kelvin-Helmholtz Rayleigh-Taylor
LHV	Lower Heating Value
NDDF	Natural Gas Diesel Dual Fuel
NG	Natural Gas
NI	National Instrument
NO_x	Nitrogen Oxides
PFI	Port Fuel Injection
PM	Particulate Matter
PPRR	Peak Pressure Rise Rate
PW	Pulse Width
PWR	Pulse Width Ratio
RPM	Revolution Per Minute
SOC	Start Of Combustion
SODI	Start Of Diesel Injection
UHC	Unburned Hydrocarbon
ULSD	Ultra-Low Sulfur Diesel

References

[1] United Nations, The Paris Agreement. Http//UnfcccInt/Files/Essential Background/Convention Appl Pdf/English _ Paris _ AgreementPdf 2015.

[2] Canadian Environmental Sustainability Indicators, Progress towards Canada's greenhouse gas emissions reduction target 2019.

[3] Musculus MPBB, Miles PC, Pickett LM. Conceptual models for partially premixed low-temperature diesel combustion. vol. 39. Elsevier Ltd; 2013. https://doi.org/10.1016/j.pecs.2012.09.001.

[4] Senecal PK, Leach F. Diversity in transportation: Why a mix of propulsion technologies is the way forward for the future fleet. Results Eng 2019;4:100060. https://doi.org/10.1016/j.rineng.2019.100060.

[5] Khandal S V., Banapurmath NR, Gaitonde VN, Hiremath SS. Paradigm shift from mechanical direct injection diesel engines to advanced injection strategies of diesel homogeneous charge compression ignition (HCCI) engines- A comprehensive review. Renew Sustain Energy Rev 2017;70:369–84. https://doi.org/10.1016/j.rser.2016.11.058.

[6] Lee S, Kim C, Lee S, Oh S, Kim J, Lee J. Characteristics of non-methane hydrocarbons and methane emissions in exhaust gases under natural-gas/diesel dual-fuel combustion. Fuel 2021;290:120009. https://doi.org/10.1016/j.fuel.2020.120009.

[7] Yang B, Ning L, Liu B, Huang G, Cui Y, Zeng K. Comparison study the particulate matter characteristics in a diesel/natural gas dual-fuel engine under different natural gas-air mixing operation conditions. Fuel 2021;288:119721. https://doi.org/10.1016/j.fuel.2020.119721.

[8] Annual Energy Outlook 2019 with projections to 2050. US Energy Inf Agency 2019.

[9] Ahmad Z, Kaario O, Karimkashi S, Qiang C, Vuorinen V, Larmi M. Effects of ethane addition on diesel-methane dual-fuel combustion in a heavy-duty engine. Fuel 2021;289:119834. https://doi.org/10.1016/j.fuel.2020.119834.

[10] Yousefi A, Guo H, Birouk M, Liko B, Lafrance S. Effect of post-injection strategy on greenhouse gas emissions of natural gas / diesel dual-fuel engine at high load conditions. Fuel 2021;290:120071. https://doi.org/10.1016/j.fuel.2020.120071.

[11] Wang Z, Zhang F, Xia Y, Wang D, Xu Y, Du G. Combustion phase of a diesel/natural gas dual fuel engine under various pilot diesel injection timings. Fuel 2021;289:119869. https://doi.org/10.1016/j.fuel.2020.119869.

[12] Pathak SK, Nayyar A, Goel V. Optimization of EGR effects on performance and emission parameters of a dual fuel (Diesel + CNG) CI engine: An experimental investigation. Fuel 2021;291:120183. https://doi.org/10.1016/j.fuel.2021.120183.

[13] Kim W, Park C, Bae C. Characterization of combustion process and emissions in a natural gas/diesel dual-fuel compression-ignition engine. Fuel 2021;291:120043. https://doi.org/10.1016/j.fuel.2020.120043.

[14] Wu Z, Han Z. Micro-GA optimization analysis of the effect of diesel injection strategy on natural gas-diesel dual-fuel combustion. Fuel 2020;259:116288. https://doi.org/10.1016/j.fuel.2019.116288.

[15] Yousefi A, Guo H, Birouk M. An experimental and numerical study on diesel injection split of a natural gas/diesel dual-fuel engine at a low engine load. Fuel 2018;212. https://doi.org/10.1016/j.fuel.2017.10.053.

[16] Yousefi A, Guo H, Birouk M. Effect of diesel injection timing on the combustion of natural gas/diesel dual-fuel engine at low-high load and low-high speed conditions. Fuel 2019;235. https://doi.org/10.1016/j.fuel.2018.08.064.

[17] Li M, Wei Z, Liu X, Wang X, Zhang Q, Li Z. A numerical investigation on the effects of gaseous fuel composition in a pilot ignited direct injection natural gas engine. Energy 2021;217:119467. https://doi.org/10.1016/j.energy.2020.119467.

[18] Lee S, Kim C, Lee S, Lee J, Kim J. Diesel injector nozzle optimization for high CNG substitution in a dual-fuel heavy-duty diesel engine. Fuel 2020;262:116607. https://doi.org/10.1016/j.fuel.2019.116607.

[19] Liu J, Ma B, Zhao H. Combustion parameters optimization of a diesel/natural gas dual fuel engine using genetic algorithm. Fuel 2020;260:116365. https://doi.org/10.1016/j.fuel.2019.116365.

[20] Guo H, Liko B, Littlejohns J. Combustion and greenhouse gas emissions of a natural gas - Diesel dual fuel engine at low and high load conditions. ASME 2019 Intern Combust Engine Div Fall Tech Conf ICEF 2019 2019. https://doi.org/10.1115/ICEF2019-7124.

[21] Chen Y, Zhu Z, Chen Y, Huang H, Zhu Z, Lv D, et al. Study of injection pressure couple with EGR on

484 combustion performance and emissions of natural gas-diesel dual-fuel engine. Fuel 2020;261:116409.
485 https://doi.org/10.1016/j.fuel.2019.116409.

486 [22] Zirngibl S, Wachtmeister G. Extensive Investigation of a Common Rail Diesel Injector Regarding Injection
487 Characteristics and the Resulting Influences on the Dual Fuel Pilot Injection Combustion Process. SAE Tech
488 Pap 2016. https://doi.org/10.4271/2016-01-0780.

489 [23] Yousefi A, Guo H, Birouk M, Liko B. On greenhouse gas emissions and thermal efficiency of natural
490 gas/diesel dual-fuel engine at low load conditions: Coupled effect of injector rail pressure and split
491 injection. Appl Energy 2019;242. https://doi.org/10.1016/j.apenergy.2019.03.093.

492 [24] Huang H, Zhu Z, Chen YYY, Chen YYY, Lv D, Zhu J, et al. Experimental and numerical study of multiple
493 injection effects on combustion and emission characteristics of natural gas–diesel dual-fuel engine. Energy
494 Convers Manag 2019;183:84–96. https://doi.org/10.1016/j.enconman.2018.12.110.

495 [25] Bartolucci L, Cordiner S, Mulone V, Krishnan SR, Srinivasan KK. A Computational Investigation of the Impact
496 of Multiple Injection Strategies on Combustion Efficiency in Diesel-Natural Gas Dual-Fuel Lowerature
497 Combustion Engines. J Energy Resour Technol Trans ASME 2019;143:1–14.
498 https://doi.org/10.1115/1.4047887.

499 [26] Guo H, Liko B, Neill WS. EFFECT OF DIESEL INJECTION SPLIT ON COMBUSTION AND EMISSIONS
500 PERFORMANCE OF A NATURAL GAS – DIESEL DUAL FUEL ENGINE AT A LOW LOAD CONDITION 2018:1–10.

501 [27] Aksu C, Kawahara N, Tsuboi K, Kondo M, Tomita E. Extension of PREMIER combustion operation range
502 using split micro pilot fuel injection in a dual fuel natural gas compression ignition engine: A performance-
503 based and visual investigation. Fuel 2016;185:243–53. https://doi.org/10.1016/j.fuel.2016.07.120.

504 [28] Yang B, Duan Q, Liu B, Zeng K. Parametric investigation of low pressure dual-fuel direct injection on the
505 combustion performance and emissions characteristics in a RCCI engine fueled with diesel and CH4. Fuel
506 2020;260:116408. https://doi.org/10.1016/j.fuel.2019.116408.

507 [29] You J, Liu Z, Wang Z, Wang D, Xu Y. Impact of natural gas injection strategies on combustion and emissions

of a dual fuel natural gas engine ignited with diesel at low loads. Fuel 2020;260:116414. https://doi.org/10.1016/j.fuel.2019.116414.

[30] Park H, Shim E, Bae C. Expansion of low-load operating range by mixture stratification in a natural gas-diesel dual-fuel premixed charge compression ignition engine. Energy Convers Manag 2019;194:186–98. https://doi.org/10.1016/j.enconman.2019.04.085.

[31] Yang B, Zeng K. Effects of natural gas injection timing and split pilot fuel injection strategy on the combustion performance and emissions in a dual-fuel engine fueled with diesel and natural gas. Energy Convers Manag 2018;168:162–9. https://doi.org/10.1016/j.enconman.2018.04.091.

[32] Walker NR, Wissink ML, DelVescovo DA, Reitz RD. Natural gas for high load dual-fuel reactivity controlled compression ignition in heavy-duty engines. J Energy Resour Technol Trans ASME 2015;137:1–7. https://doi.org/10.1115/1.4030110.

[33] Pettinen R, Kaario O, Larmi M. Dual-Fuel Combustion Characterization on Lean Conditions and High Loads. SAE Tech Pap 2017;2017-March. https://doi.org/10.4271/2017-01-0759.

[34] Guo H, Liko B. Injector tip temperature and combustion performance of a natural gas – Diesel dual fuel engine at medium and high load conditions. ASME 2018 Intern Combust Engine Div Fall Tech Conf ICEF 2018 2018;1. https://doi.org/10.1115/ICEF2018-9664.

[35] Johnson DR, Heltzel R, Nix AC, Clark N, Darzi M. Greenhouse gas emissions and fuel efficiency of in-use high horsepower diesel, dual fuel, and natural gas engines for unconventional well development. Appl Energy 2017;206:739–50. https://doi.org/10.1016/j.apenergy.2017.08.234.

[36] Yousefi A, Guo H, Birouk M. Effect of swirl ratio on NG/diesel dual-fuel combustion at low to high engine load conditions. Appl Energy 2018;229. https://doi.org/10.1016/j.apenergy.2018.08.017.

[37] Rimmer JET, Johnson SL, Clarke A. An experimental study into the effect of the pilot injection timing on the performance and emissions of a high-speed common-rail dual-fuel engine. Proc Inst Mech Eng Part D J Automob Eng 2014;228:929–42. https://doi.org/10.1177/0954407013506180.

[38] Yousefi A, Birouk M, Guo H. On the Variation of the Effect of Natural Gas Fraction on Dual-Fuel Combustion of Diesel Engine Under Low-to-High Load Conditions. Front Mech Eng 2020;6. https://doi.org/10.3389/fmech.2020.555136.

[39] Greenhouse Gas Emissions and Fuel Efficiency Standards for Medium- and Heavy-Duty Engines and Vehicles— Phase 2. US EPA 40 CFR Parts 9, 22, 85 2016.

[40] Han J, Sonntag D. Update of Engine Categories, Emission Rates and Speciation Profiles for Tier-4 Nonroad Compression Ignition Engines. MOVES Rev Work Group, Us EPA 2017.

[41] Richards K.J. SPK and PE. Converge Manual. Converg (Version 24) Manual," Converg Sci Inc, Madison, Wisconsin, USA 2017.

[42] Yousefi A, Guo H, Birouk M. Effect of diesel injection timing on the combustion of natural gas/diesel dual-fuel engine at low-high load and low-high speed conditions. Fuel 2019;235:838–46. https://doi.org/10.1016/j.fuel.2018.08.064.

[43] Yousefi A, Guo H, Birouk M, Liko B. On greenhouse gas emissions and thermal efficiency of natural gas/diesel dual-fuel engine at low load conditions: Coupled effect of injector rail pressure and split injection. Appl Energy 2019;242:216–31. https://doi.org/10.1016/j.apenergy.2019.03.093.

[44] Yousefi A, Guo H, Birouk M. Split diesel injection effect on knocking of natural gas/diesel dual-fuel engine at high load conditions. Appl Energy 2020;279:115828. https://doi.org/10.1016/j.apenergy.2020.115828.

[45] Rahimi A, Fatehifar E, Saray RK. Development of an optimized chemical kinetic mechanism for homogeneous charge compression ignition combustion of a fuel blend of n-heptane and natural gas using a genetic algorithm. Proc Inst Mech Eng Part D J Automob Eng 2010;224:1141–59. https://doi.org/10.1243/09544070JAUTO1343.

[46] Beale JC, Reitz RD. Modeling spray atomization with the Kelvin-Helmholtz/Rayleigh-Taylor hybrid model. At Sprays 1999;9:623–50.

[47] Senecal PK, Richards KJ, Pomraning E, Yang T, Dai MZ, McDavid RM, et al. A New Parallel Cut-Cell Cartesian

CFD Code for Rapid Grid Generation Applied to In-Cylinder Diesel Engine Simulations 2007;2007:776–90. https://doi.org/10.4271/2007-01-0159.

[48] Wijeyakulasuriya S. Multidimensional Modeling and Validation of Dual-Fuel Combustion in a Large Bore Medium Speed Diesel Engine. Proc ASME 2015 Intern Combust Engine Div Fall Tech Conf ICEF2015 Novemb 8-11, 2015, Houston, TX, USA 2015:1–14.